Photodynamics of Red Fluorescent Proteins Studied by Fluorescence Correlation Spectroscopy

ARTICLE *in* BIOPHYSICAL JOURNAL · FEBRUARY 2004

Impact Factor: 3.97 · DOI: 10.1016/S0006-3495(04)74114-4 · Source: PubMed

5 AUTHORS, INCLUDING:

Sergey Ivanchenko
Ludwig-Maximilians-University of Munich
33 PUBLICATIONS **1,029** CITATIONS
SEE PROFILE

Carlheinz Röcker
Universität Ulm
49 PUBLICATIONS **2,419** CITATIONS
SEE PROFILE

Photodynamics of Red Fluorescent Proteins Studied by Fluorescence Correlation Spectroscopy

Andreas Schenk,* Sergey Ivanchenko,* Carlheinz Röcker,* Jörg Wiedenmann,† and G. Ulrich Nienhaus*‡
*Department of Biophysics, and †Department of General Zoology and Endocrinology, University of Ulm, Ulm, Germany; and
‡Department of Physics, University of Illinois at Urbana-Champaign, Urbana, Illinois

ABSTRACT Red fluorescent proteins are important tools in fluorescence-based life science research. Recently, we have introduced eqFP611, a red fluorescent protein with advantageous properties from the sea anemone *Entacmaea quadricolor*. Here, we have studied the submillisecond light-driven intramolecular dynamics between bright and dark states of eqFP611 and, for comparison, drFP583 (DsRed) by using fluorescence correlation spectroscopy on protein solutions. A three-state model with one dark and two fluorescent states describes the power-dependence of the flickering dynamics of both proteins at different excitation wavelengths. It involves two light-driven conformational transitions. We have also studied the photodynamics of individual (monomeric) eqFP611 molecules immobilized on surfaces. The flickering rates and dark state fractions of eqFP611 bound to polyethylene glycol-covered glass surfaces were identical to those measured in solution, showing that the bound FPs behaved identically. A second, much slower flickering process was observed on the 10-ms timescale. Deposition of eqFP611 molecules on bare glass surfaces yielded bright fluorescence without any detectable flickering and a >10-fold decreased photobleaching yield. These observations underscore the intimate connection between protein motions and photophysical processes in fluorescent proteins.

INTRODUCTION

Since the successful cloning of the green fluorescent protein from the jellyfish *Aequorea victoria* (avGFP) in 1992 (Prasher et al., 1992), fluorescent proteins (FPs) and their mutants have revolutionized life science research as labels, noninvasive markers of gene expression, reporters of environmental conditions in living cells, and many other applications (for a review see Tsien, 1998). In recent years, FPs have also been identified in Anthozoa species (Matz et al., 1999; Wiedenmann et al., 2000, 2002; Nienhaus et al., 2003). Some of these novel FPs have interesting properties, most importantly, red fluorescence emission. In our group, we have cloned and characterized a far-red fluorescent protein from the sea anemone *Entacmaea quadricolor*, eqFP611, which features fast chromophore maturation and low oligomerization tendency (Wiedenmann et al., 2002). In the meantime, a preliminary x-ray structure of this protein has also been reported (Nienhaus et al., 2003).

The polypeptide chain of FPs folds into a cylinder of ~40 Å length and 30 Å diameter, with 11 β-strands forming a nearly perfect β-barrel. It encloses a central helix that contains the fluorophore (Ormö et al., 1996; Yang et al., 1996; Wall et al., 2000; Nienhaus et al., 2003). This fold conveys exceptional stability to the protein, as judged by its resistance to denaturants and proteases (Tsien, 1998) as well as high melting temperatures in thermal denaturation studies (Ward, 1982). The remarkable rigidity of the overall protein framework of GFP has been confirmed with molecular dynamics simulations (Helms et al., 1999). The fluorophore is tightly packed and hydrogen-bonded in a rigid cage inside the β-barrel, where it is protected from the bulk solvent. The rigid enclosure of the fluorophore is apparently a prerequisite for the chromophore to fluoresce with high quantum yield. Indeed, denatured FPs or bare chromophores in aqueous solution do not fluoresce at all at room temperature. These preparations become highly fluorescent, however, after cooling to cryogenic temperatures in glass-forming liquids, which suppresses conformational dynamics (Niwa et al., 1996). Fluorescence quantum yields vary widely for different FPs and mutants, indicating that the chromophore is exquisitely sensitive to its immediate protein environment (Kummer et al., 1998, 2000). Apparently, internal conversion gains importance with increasing conformational flexibility in the fluorophore cage. Photoisomerization of the hydrogen-bonding network and bond rotation within the chromophore have been suggested as mechanisms promoting nonradiative excitation decay (Voityuk et al., 1998; Weber et al., 1999; Kummer et al., 2002).

Under physiological conditions, protein molecules are known to fluctuate among a large number of conformational substates that may differ slightly in their structural properties (Nienhaus and Young, 1996; Nienhaus et al., 1997). These substates may have markedly different functional properties, however, as is well-known from kinetic studies on many different proteins (Frauenfelder et al., 1991; Ehrenstein and Nienhaus, 1992; McMahon et al., 1998; Kriegl et al., 2002). Considering the exquisite dependence of the FP chromophore on the properties of its cage, it comes as no surprise that all known FPs exhibit time-dependent fluctuations of their fluorescence emission, which suggests that either thermally induced or light-driven transitions occur between conformations with distinctly different emission properties (for

Submitted July 14, 2003, and accepted for publication August 15, 2003.

Address reprint requests to Gerd Ulrich Nienhaus, Dept. of Biophysics, University of Ulm, 89069 Ulm, Germany. Tel.: 49-731-502-3050; Fax: 49-731-502-3059; E-mail: uli@uiuc.edu.

0006-3495/04/01/384/11 $2.00

instance, fluorescence quantum yield). This flickering is completely obscured when many FP molecules are observed simultaneously. Single-molecule techniques, however, can detect photodynamics over a wide range of timescales. Flickering on timescales faster than milliseconds was evident in experiments using fluorescence correlation spectroscopy (FCS) on avGFP mutants (Haupts et al., 1998; Widengren et al., 1999; Heikal et al., 2000; Jung et al., 2000; Schwille et al., 2000), drFP583, a red fluorescent protein from *Discosoma* (also known as DsRed) (Heikal et al., 2000; Malvezzi-Campeggi et al., 2001), and eqFP611 (Wiedenmann et al., 2002). On/off switching of the fluorescence signal on timescales from milliseconds to seconds, depending on excitation intensity and protein environment, was noticed in single-molecule experiments on several avGFP mutants (Dickson et al., 1997; Jung et al., 1998; Peterman et al., 1999; Garcia-Parajo et al., 2000).

Detailed studies of flickering processes in FPs are most interesting in various respects. They provide insights into the photophysics and photochemistry of the fluorophore and its coupling to the protein matrix. Moreover, the fluorescence emission can be used as a convenient tool to study interconversions among conformational substates in these proteins. Based on a thorough understanding of fluorophore-protein interactions, it will become possible to rationally design FPs with superior emission properties and less flickering in the quest for optimal fluorescent marker tools in the life sciences. In this work, we present a detailed characterization of the flickering dynamics of eqFP611 measured with FCS both on solution samples and on surface-immobilized single molecules. A kinetic model with three distinguishable species is introduced, which consistently describes the excitation intensity dependence of the flickering in FCS data on eqFP611 and drFP583 (DsRed) at different excitation wavelengths.

MATERIALS AND METHODS

Protein preparation

eqFP611 was cloned as described (Wiedenmann et al., 2002). The drFP583 clone was a kind gift from Dr. Sergey A. Lukyanov (Russian Academy of Sciences, Moscow, Russia). The clone of the avGFP mutant S65T was obtained from C. Kaether (European Molecular Biology Laboratory, Heidelberg, Germany). All proteins were expressed in *E. coli* (BL21 DE3) and purified using a Talon metal affinity resin (BD Biosciences CLONTECH, Palo Alto, CA) and gel filtration (Superdex 200, Äkta-System, Amersham Pharmacia, Little Chalfont, UK) (Wiedenmann et al., 2002).

FCS measurements on protein solutions

FCS experiments were performed with 2 nM protein dissolved in Tris buffer (50 mM, 300 mM NaCl, pH 8.5) using a confocal microscope of our own design. Light from an Ar^+/Kr^+-ion laser (modified model 164, Spectra-Physics, Mountain View, CA) was reflected by a dichroic mirror (EGFP: Q495LP; red FPs: Q525LP or 575DCXR, AHF, Tübingen, Germany) and focused on the sample with a water-immersion objective (UPLAPO 60×/1.2 W, Olympus, Hamburg, Germany) in an inverted microscope (Axiovert 35, Zeiss, Göttingen, Germany). The emitted fluorescence photons were collected by the same objective, passed through the dichroic mirror and focused with a lens ($f = 150$ mm) onto a confocal pinhole. After passing through the pinhole, the light was divided into two channels with a 50% beam splitter and detected by two avalanche photodiodes (SPCM-AQR-14, PerkinElmer, Fremont, CA). For EGFP, an emission bandpass with 535-nm center wavelength and 70-nm width (535/70, AHF) was used in front of the beam splitter; for the red FPs, the observed spectral band was limited either by a dichroic mirror (640 DCXXR, AHF) in combination with a longpass filter (HQ 700/300, AHF) or a bandpass filter (HQ 665/170, AHF). The outputs of the detection channels were cross-correlated in a digital correlator (ALV-5000/E, ALV, Langen, Germany). Frequent control measurements with rhodamine 6G solutions ensured the proper alignment of the confocal optics and the absence of artifacts in the FCS autocorrelation function (ACF) (Hess and Webb, 2002). For optimal sensitivity toward the reaction and diffusion components in the ACF (vide infra), the measurements were performed with different confocal volumes (defined by integrating a three-dimensional Gaussian volume), ranging from 0.5 to 10 fl. These were achieved by varying the size of the confocal pinhole (80–300 μm) and the extent to which the back aperture plane of the objective lens was filled by the excitation laser beam, using a diaphragm and a telescope in the excitation light path. Excitation rates were calculated on the basis of the laser power measured at the entrance port of the microscope, the attenuation by the dichroic mirror, a 95%/5% beam-splitting mirror and the objective lens, and the extinction coefficients of drFP583 (Campbell et al., 2002) and eqFP611 (Wiedenmann et al., 2002), as described in the Appendix.

For measurements of rotational correlation times, small confocal volumes (~1 fl), high excitation rates (~5 MHz), and long data acquisition times (30 min) were used to optimize S/N ratios on the nanosecond timescale. All measurements reported in this article were carried out in our temperature-controlled laboratory at 22°C.

Single-molecule FCS

Single-molecule experiments on surface-immobilized proteins have the advantage that the observation time is not limited by diffusion, but rather by the inevitable photobleaching of the fluorophore. For meaningful results, the biomolecules should be attached to surfaces that provide homogeneous environments which exert only minimal influence on their intrinsic properties. In this work, we have immobilized eqFP611 on glass coverslips coated with PEG (polyethylene glycol) polymer chains. The coverslips were silanized and amino-functionalized with Vectabond (Vector Laboratories, Burlingame, CA) according to the manufacturer's protocol. Subsequently, they were incubated with a solution of 100 mg/ml PEGs in 50 mM Na_2CO_3 buffer (pH 8.2) for 90 min in the dark. The PEG chains carried a succinimidyl function on one end to bind to the amino groups on the silanized glass surfaces. In 1% of the chains, the other end was biotinylated for attachment of proteins via a streptavidin-biotin link so as to obtain a sparse coverage with biotin anchors on the PEG-coated surface. To this end, we used a mixture of 1% biotinylated PEG (Biotin-PEG-NHS MW 3400, Nektar Therapeutics, Huntsville, AL) and 99% PEG (mPEG-SPA MW 5000, Nektar Therapeutics). The x-ray structure of eqFP611 shows two surface-exposed cysteines (Nienhaus et al., 2003). These were biotinylated using biotin-maleimide (Sigma-Aldrich, St. Louis, MO) according to standard labeling procedures (Hermanson, 1996). For protein attachment, the PEG surfaces were incubated with a 10-μg/ml streptavidin solution (Sigma-Aldrich) and afterwards with a 100-pM solution of biotinylated eqFP611 for 10 min each. The protein solution was subsequently flushed out with plain buffer.

To investigate the individual protein molecules attached to the PEG surfaces, we used the same setup as for solution FCS, using the 665/170 bandpass filter and an 80-μm pinhole. The samples were mounted on a piezoelectric scanning stage (Tritor 102 Cap, Piezosysteme Jena, Jena, Germany). 18 × 18-μm^2-sized regions of the sample were scanned with

a resolution of 128 × 128 pixels and an integration time of 5 ms/pixel. For the measurement of time trajectories, immobilized protein molecules were localized by scanning, and their fluorescence emission was subsequently recorded with 625-ns binwidth until photobleaching occurred.

EXPERIMENTAL RESULTS

Spectroscopic properties

Fig. 1 shows normalized excitation and emission spectra of eqFP611 and drFP583. The excitation spectra of the two proteins are similar, peaking at 559 and 558 nm, respectively. The higher (relative) excitation probability of drFP583 at shorter wavelengths is caused by stronger vibronic coupling to modes ~1300 cm^{-1} (He et al., 2002; Kruglik et al., 2002), as seen from the peak at 520 nm, and by incomplete maturation of the green precursor chromophore, which is responsible for the surplus in excitability <500 nm. The emission band of drFP583 is Stokes-shifted by 25 nm and shows a vibronic sideband as a shoulder near 630 nm. The emission from eqFP611 is shifted by 52 nm and much broader than the one of drFP583; no vibronic structure can be discerned.

FCS measurements in solution

FCS curves were measured for eqFP611 and drFP583 with excitation rates ranging from 0.1 to 10 MHz and varying confocal geometries. A typical data set of eqFP611, with fluorescence excitation at 514 nm, is plotted in Fig. 2. The decay of the autocorrelation functions exhibits two steps. The first one occurs on sub-ms timescales and shifts to shorter times with increasing excitation power. It is independent of the size of the confocal volume (at constant excitation rate) and, therefore, assigned to an internal, light-induced process. This phenomenon is commonly called flickering of the fluorescence emission. The second decay varies with the size of the confocal volume and represents translational diffusion of the molecules through the volume.

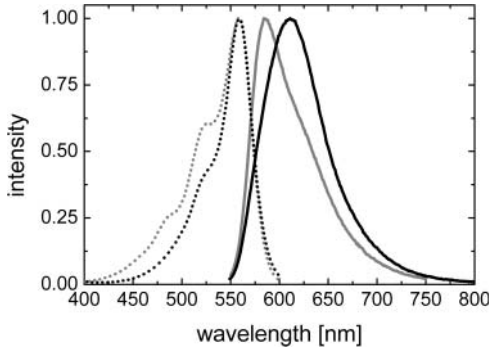

FIGURE 1 Fluorescence excitation (*dotted lines*) and emission spectra (*solid lines*) of eqFP611 (*black lines*) and drFP583 (*gray lines*). Excitation spectra were recorded at 611 nm; emission spectra were taken with excitation at 530 nm (drFP583) and 546 nm (eqFP611).

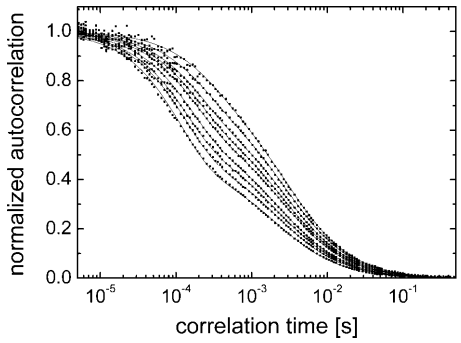

FIGURE 2 Normalized fluorescence correlation functions of eqFP611 excited at 514 nm. Excitation rates were varied in the range from 0.2 (*rightmost curve*) to 3.7 MHz (*leftmost curve*). The solid lines are fits with Eq. 1.

In this study, we have employed variation of the confocal geometry not only to unambiguously distinguish between diffusion and reaction, but also to study the photodynamics over a wide range of excitation rates. By using large confocal volumes, the diffusional decay can be shifted to longer times, which helps to separate the reaction and diffusion steps. This is particularly important at lower excitation rates (Fig. 2). Smaller volumes, however, are helpful for achieving high excitation rates.

In the simplest way, the FCS data can be analyzed by assuming freely diffusing molecules undergoing a unimolecular reaction between two states with different emissivity. For this case, the ACF is given by (Elson and Magde, 1974; Lamb et al., 2000)

$$G(\tau) = \frac{2^{-3/2}}{N} \frac{1}{1+\tau/\tau_D} \frac{1}{\sqrt{1+(r_0^2/z_0^2)(\tau/\tau_D)}} \times \left[1 + \frac{F}{1-F}\exp(-\lambda\tau)\right]. \quad (1)$$

Here, N is the time-averaged number of molecules in the confocal volume, τ_D represents the diffusional correlation time of a molecule through the focus, and r_0 and z_0 are the radial and axial dimensions of the observation volume over which the intensity decays by a factor of $1/e^2$ (~0.135), respectively. F denotes the mean fraction of molecules in the dark state, and λ is the apparent flicker rate.

Excellent agreement was achieved by fitting the data with Eq. 1, as seen from the lines through the data points in Fig. 2. For each data set, diffusion times τ_D, dark state fractions F, and flicker rates λ were determined as a function of the incident laser power. A procedure was developed by which the (average) power density and excitation rate can be calculated from the incident laser power for varying confocal geometries, as is described in the Appendix. This allowed us to condense several data sets taken on the same protein at the same excitation wavelength, but with different confocal geometries, into a single curve.

The fit of the ACFs yields diffusional correlation times, τ_D, which can be converted into (apparent) diffusion coefficients. We have used rhodamine 6G as a conversion standard ($D = 280\ \mu m^2/s$; Magde et al., 1974). Fig. 3 shows a plot of these data as a function of the power density for the two red FPs. Data on EGFP (GFP mutant S65T/F64L) are included for comparison. The linear increase of the apparent diffusion coefficient with excitation power density is, of course, an artifact caused by photodynamic processes (flickering, bleaching) on the timescale of diffusion. It is evident from the data that diffusion coefficients can only be determined reliably from FCS data by extrapolation to zero power density; these values are compiled in Table 1. EGFP diffuses faster than eqFP611, and drFP583 is the slowest of the three proteins. The diffusion coefficients depend on the molecular sizes of the proteins; they are related to the hydrodynamic radii by the Stokes-Einstein relation,

$$D = \frac{k_B T}{6\pi\eta r_h}. \quad (2)$$

Using this relation, we can calculate ratios of hydrodynamic volumes for EGFP, eqFP611, and drFP583 as 1 : 2.9 : 9.3.

FCS analysis of the rotational correlation decay yields rotational diffusion coefficients, $\tau_{rot} = D_{rot}/6$. They are related to the molecular volumes by

$$D_{rot} = \frac{k_B T}{6\eta V_h}. \quad (3)$$

Fig. 4 shows FCS data of the three proteins in the time range from 10 to 500 ns. For comparison, we have also studied rhodamine 6G. Its rotational correlation time of 200 ps (Olivini et al., 2001) is outside the time window of our instrument, and thus, its ACF is constant down to 10 ns. The ACF of EGFP, however, increases at <40 ns, consistent with an exponential decay with a relaxation time of 16 ns (*dashed line*). For the two red fluorescent proteins, the ACFs increase already at <200 ns, in agreement with an exponential decay with relaxation time 64 ns (*dashed line*).

TABLE 1 Parameters of translational and rotational diffusion of EGFP, eqFP611, and drFP583 obtained by FCS

Protein	Exc. wavelength [nm]	Transl. diff. coeff. [$\mu m^2/s$]	Rot. corr. time [ns]
EGFP	488	63 ± 3	~16
eqFP611	514	44 ± 2	~64
drFP583	514	30 ± 2	~64

Information about the photophysical processes occurring during diffusion of the proteins in the sensitive volume is contained in the two parameters, dark state fraction F and flicker rate λ. Their dependencies on excitation power were carefully examined for three different excitation wavelengths, 488, 514, and 531 nm. These data are plotted in Fig. 5 against the excitation rate k_{ex} for eqFP611 and drFP583. Both F and λ show a pronounced dependence on the excitation rate, clearly indicating that flickering is light-driven. Whereas λ increases monotonically, the dark state fraction exhibits a maximum at ~2 MHz (eqFP611) and ~1 MHz (drFP583), respectively. For both proteins, the dark state fractions are similar for excitation at 514 and 531 nm, but significantly smaller for excitation at 488 nm. This observation further underscores the light-driven nature of the flickering.

FCS on immobilized proteins

In solution FCS, the diffusional decay of the autocorrelation function limits the studies of the reaction dynamics to timescales faster or at least on the order of the diffusional correlation time τ_D. To extend our investigation beyond this limit, we recorded the fluorescence emission from individual eqFP611 molecules immobilized on PEG surfaces, using an average excitation rate of 0.14 MHz.

Fig. 6 *a* shows a confocal scan image of immobilized eqFP611 molecules. Fluorescence time trajectories of in-

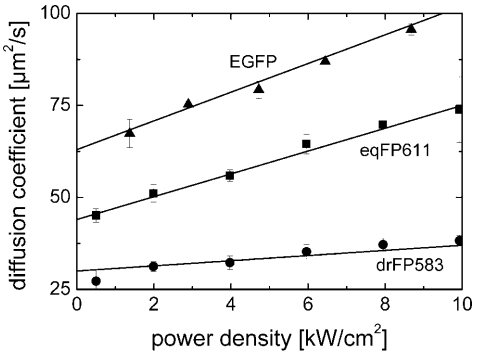

FIGURE 3 Apparent diffusion coefficient of eqFP611 (*squares*), drFP583 (*circles*), and EGFP (*triangles*) versus normalized power density with excitation at 514 nm (eqFP611 and drFP583) and 488 nm (EGFP). The intersections of the fitted lines with the *y* axis yield the diffusion coefficients of the proteins.

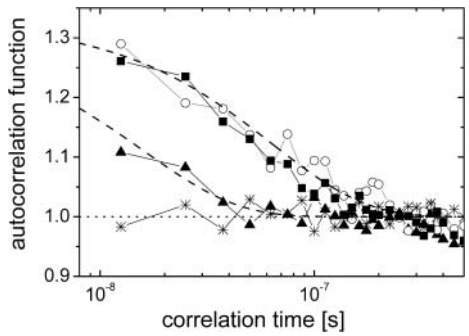

FIGURE 4 Rotational correlation functions of EGFP (*triangles*), eqFP611 (*squares*), and drFP583 (*circles*). A measurement with rhodamine 6G is included for comparison (*asterisks*). Exponentials with time constants of 16 ns and 64 ns are shown as dashed lines.

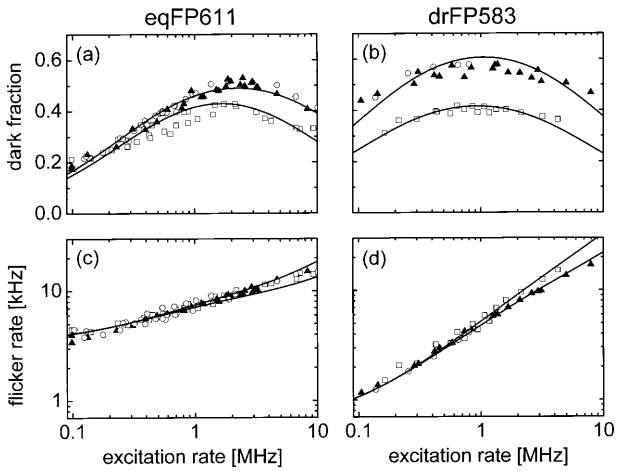

FIGURE 5 Dark state fractions (*top row*) and flicker rate (*bottom row*) of eqFP611 (*left column*) and drFP583 (*right column*) versus excitation rate, measured at three different excitation wavelengths: 488 nm (*unfilled squares*), 514 nm (*triangles*), and 531 nm (*circles*). The solid lines are the result of fits using Eqs. 6 and 8. For fitting, the essentially identical data sets with excitation at 514 nm and 531 nm were combined.

dividual molecules were recorded with a binning time of 625 ns. Three typical examples are shown in Fig. 6 *c*. The molecules emit over several hundred ms. There are, however, extended periods during which they are completely nonemitting (background level!). Note that, at the plot resolution of 1 ms, the fast flickering observed in FCS is only visible as excess noise during steady periods of high emission. Finally, the molecules fall victim to photodestruction; the intensity drops to the background level in a single step, confirming (posthumously) that the emission derived from a single fluorophore. Fig. 6 *b* shows a histogram of the observed numbers of photons from 160 eqFP611 molecules. The solid line is an exponential fit, yielding a $1/e$ decay at 1234 ± 88 detected photons. Estimating the overall detection efficiency of the system as ~5%, this decay corresponds to 24,200 emitted photons. Taking the fluorescence quantum yield of 0.45 (at room temperature) into account (Wiedenmann et al., 2002), a total of ~54,000 excitations occur on average before photobleaching, corresponding to a yield of photobleaching $\Phi_B \approx 1.9 \times 10^{-5}$.

To characterize the photodynamics, ACFs were calculated from individual time trajectories. An example is shown in Fig. 7 *a* (*unfilled symbols*). All ACFs exhibit a clear step at ~300 μs, which does not decay to 0, however, indicating that slower correlations are present. Because of the limited signal/noise ratio, we averaged 76 single-molecule ACFs to unambiguously characterize the slower process. (Fig. 7 *b*). The average ACF clearly exhibits a two-step decay, showing an additional flickering process with smaller amplitude at longer timescales. It can be described very well with a sum of two exponentials,

$$G(\tau) = A_1 \exp[-\lambda_1 \tau] + A_2 \exp[-\lambda_2 \tau], \qquad (4)$$

with amplitude $A_1 = 0.18 \pm 0.01$, flicker rate $\lambda_1 = (3500 \pm 100)$ Hz, and $A_2 = 0.080 \pm 0.001$ and $\lambda_2 = (105 \pm 5)$ Hz. After the identification of the slow process, we fitted all 76 individual ACFs, keeping λ_2 fixed at 105 Hz. Fig. 7 *c* shows histograms of the dark fraction, $F = A_1/(1 + A_1)$, and the rate coefficient λ_1, as determined from the analysis of the individual traces. For the dark fraction, we obtained a mean, $\langle F \rangle = 0.17$, and the observed distribution can be fitted by a Gaussian peaking at (0.166 ± 0.005) with a standard deviation of (0.062 ± 0.005). For the flicker rate, $\langle \lambda \rangle = 3400$ Hz, and the Gaussian is centered at (3160 ± 60) Hz and has a standard deviation of (1170 ± 60) Hz. Note that the mean parameters are consistent with those obtained by the solution FCS data (see Fig. 5, *a* and *c*). This comparison suggests that the surface-immobilized molecules behave like the ones dissolved in buffer. Finally, we note that control experiments showed only negligible effects of photobleaching of fluorescent background on our single-molecule ACFs.

Three-state kinetic analysis of flickering from solution FCS

The dependencies of the dark state fractions and flicker rates on the excitation intensity provide clear evidence of the presence of photoactivated processes. So far, we have extracted the parameters F and λ using an ACF for a unimolecular reaction between a fluorescent and a nonfluorescent species. Within the framework of a two-state model, however, λ should be strictly linear in k_{ex} and F should saturate. The data in Fig. 5 of eqFP611 and drFP583 disagree with this expectation; λ rather depends in a power-law fashion on k_{ex} and F goes through a maximum instead of saturating. However, both proteins exhibit qualitatively the same behavior, which calls for a consistent description with a more complex kinetic scheme that involves at least three distinguishable species. For a quantitative description of the photodynamics of both eqFP611 and drFP583 with excitation at different wavelengths, we have explored all kinds of kinetic schemes. The following one was identified as the simplest that is compatible with the essential observations:

$$B \underset{k_{-1}}{\overset{\Phi_1 \cdot k_{ex}}{\rightleftharpoons}} B^* \underset{k_{-2} + \Phi_{-2} \cdot k_{ex}}{\overset{k_2}{\rightleftharpoons}} D \qquad (5)$$

In this model, we have introduced two bright states B and B^* and a third, dark state D. Interconversions between the three states can in general be thermally activated and/or light-induced, so that the rate coefficient of the latter process can be written as a product of a quantum yield Φ and the excitation rate k_{ex}. We note here that k_{ex} is an average rate; it is a somewhat ill-defined quantity because it varies considerably across the confocal volume. It was necessary to

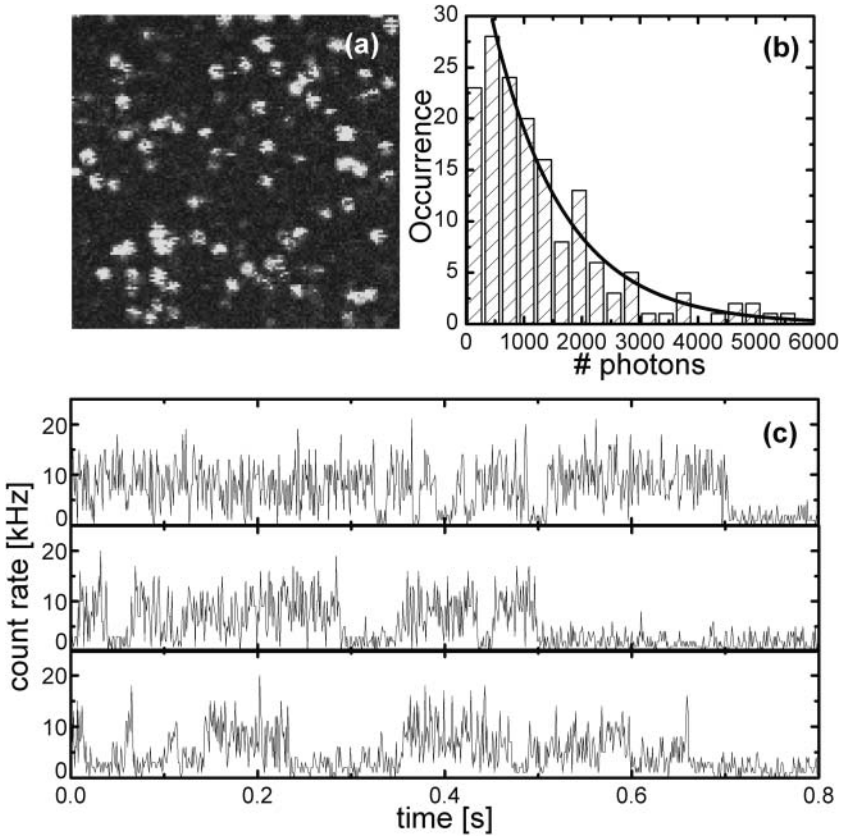

FIGURE 6 (*a*) Confocal scanning microscopy image (128 ×128 pixels, field of view 18 × 18 μm^2, 5-ms integration time per pixel, excitation rate 0.14 MHz at 514 nm) of individual eqFP611 molecules attached to a PEG-coated surface. (*b*) Histogram of the total number of photons collected from 160 individual time traces before photodestruction. An exponential fit is included as the solid line. (*c*) Typical fluorescence time trajectories of individual eqFP611 molecules (traces recorded with 625 ns and plotted with 1-ms resolution).

include two light-driven processes to reproduce the observed excitation rate-dependence of the parameters F and λ. The first one is the light-induced transition from the bright state B to the intermediate bright state B^* with quantum yield Φ_1 and rate coefficient $\Phi_1 \cdot k_{ex}$. The reverse process is treated as thermally activated, with rate coefficient k_{-1}. The transition from B^* to D is also modeled as a thermal transition, with rate coefficient k_2. The reverse transition from D to B^* contains the second light-driven process, with rate coefficient $\Phi_{-2} \cdot k_{ex}$, in addition to a thermally activated transition, with rate coefficient k_{-2}. For this kinetic scheme, the dark state fraction F and the flicker rate λ are given by

$$F = \frac{D}{D + B + B^*} = \frac{1}{(1 + P_1/k_{ex})(P_2 + P_3\,k_{ex}) + 1}, \qquad (6)$$

and

$$\lambda = \frac{1}{2}[\Phi_1(k_{ex} + P_1) + k_2(1 + P_2 + P_3\,k_{ex})] - \frac{1}{2}[(\Phi_1(k_{ex} + P_1) + k_2(1 + P_2 + P_3\,k_{ex}))^2 - 4\Phi_1 k_2((P_2 + P_3 k_{ex})(P_1 + k_{ex})k_{ex})]^{1/2}. \qquad (7)$$

Here we have introduced the parameters $P_1 = k_{-1}/\Phi_1$, $P_2 = k_{-2}/k_2$, and $P_3 = \Phi_{-2}/k_2$. The expression for λ, Eq. 7, simplifies further if the transitions between B and B^* are much faster than those between B^* and D (i.e., $\Phi_1 \cdot k_{ex} + k_{-1} \gg k_2 + k_{-2} + \Phi_{-2}\,k_{ex}$),

$$\lambda = k_2\left(\frac{\Phi_1 k_{ex}}{\Phi_1 k_{ex} + k_{-1}}\right) + (k_{-2} + \Phi_{-2}k_{ex}). \qquad (8)$$

Note that this result would also be obtained for a two-state model $B^* \leftrightarrow D$ in which the forward rate coefficient k_2 is replaced by $k_2 \cdot B^*/(B + B^*)$. This approximation is appropriate, as verified by an analysis based on the exact expression, Eq. 7.

The scheme in Eq. 5 is motivated by the following observations: the dark fraction F is observed to increase linearly with increasing excitation rate at low powers (Fig. 5, *a* and *b*). This property is incorporated in the first light-driven process, which ensures that the B^* population grows with increasing k_{ex}. Concomitantly, the dark fraction grows because state D is populated by thermal activation from B^*. Moreover, according to Eq. 8, λ does not go to zero at low power but rather approaches the thermal rate coefficient k_{-2}, independent of the excitation wavelength, as is indeed confirmed by the data in Fig. 5, *c* and *d*. At higher powers, the second light-driven process becomes important, resulting in a decrease of the dark fraction with increasing k_{ex}. This behavior can also be accounted for in a scheme with only a single-light-driven process, but with a ''dark'' state having a finite fluorescence quantum yield, as has been suggested

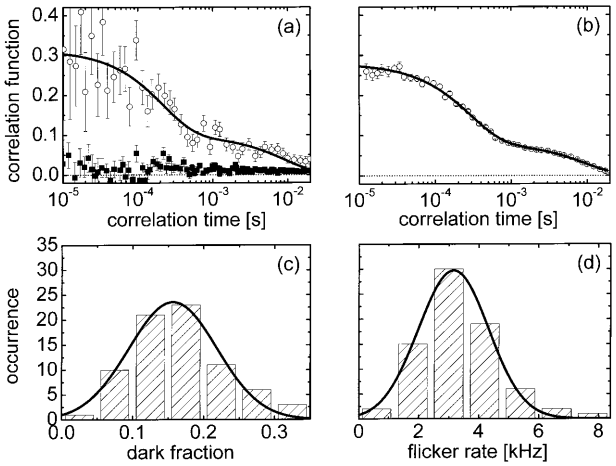

FIGURE 7 (*a*) Autocorrelation curves of individual eqFP611 molecules dried on a bare glass surface (*squares*) and immobilized on a PEG-coated surface (*circles*). The solid line represents a double-exponential fit to the data. The dotted line shows the zero level. (*b*) Average of 76 correlation functions of individual molecules immobilized on a PEG-covered surface. The solid line shows a double exponential fit to the data. Histograms of the dark fraction (*c*) and the flicker rate (*d*) are plotted for 76 molecules and fitted with Gaussian distributions.

for DsRed (Malvezzi-Campeggi et al., 2001). Note, however, that Fig. 5, *a* and *b*, displays markedly different dependencies of the dark fractions on the excitation wavelength. The maximum amplitudes and their respective excitation rates are clearly different and cannot be modeled by any scheme that includes only a single light-induced process (i.e., $\Phi_{-2} = 0$). Further support for the presence of the second light-driven process comes from the behavior of λ, which does not saturate at higher powers (see Eq. 8); it rather increases further due to the term $\Phi_{-2} \cdot k_{ex}$.

We performed fits of both F and λ at different excitation wavelengths, treating the thermal rate coefficients k_2 and k_{-2} as global parameters for all wavelengths. Since the data for excitation wavelengths 514 and 532 nm are identical within the error, these two datasets were fitted with one curve. Our model consistently describes the light intensity dependence of both dark state fraction F and flicker rate λ simultaneously for both eqFP611 and drFP583, as shown by the solid lines in Fig. 5. Within the approximation of fast preequilibrium (Eq. 8), the independent determination of all parameters is not feasible; Φ_1 and k_{-1} cannot be determined individually, but only their ratio P_1. The fit parameters and the resulting rate coefficients k_2, k_{-2}, and Φ_{-2} are compiled in Table 2.

TABLE 2 Parameters of the three-state model introduced to fit the observed excitation rate dependence of the flickering rates λ and dark fractions F of eqFP611 and drFP583 (Fig. 5)

Protein	eqFP611		drFP583	
Exc. wavelength	488 nm	514/531 nm	488 nm	514/531 nm
P_1 [MHz]	0.81 ± 0.05	0.72 ± 0.05	3.8 ± 0.4	2.6 ± 0.3
P_2*	0.60 ± 0.02		0.054 ± 0.006	
P_3 [1/MHz]	0.18 ± 0.01	0.09 ± 0.01	0.24 ± 0.02	0.13 ± 0.01
k_2 [Hz]*	5600 ± 200		10,400 ± 800	
k_{-2} [Hz]†	3360 ± 230		560 ± 100	
Φ_{-2} /10^{-3}†	1 ± 0.1	0.5 ± 0.07	2.5 ± 0.4	1.4 ± 0.2
$P_1 \cdot P_2$ [MHz]†	0.49 ± 0.05	0.43 ± 0.04	0.21 ± 0.04	0.14 ± 0.03

*Global parameters.
†Derived parameters.

DISCUSSION

Fluorescence dynamics of surface-immobilized proteins

By measuring the time dependence of the fluorescence emission of many eqFP611 molecules tethered to PEG brush surfaces under low excitation conditions (0.14 MHz), we have identified two distinct dynamic processes in the single-molecule ACFs, a fast and a slow flickering process between bright and dark states on timescales of ~300 μs and ~10 ms, respectively. The slow process is very obvious from the extended dark periods in the time traces displayed in Fig. 6 *c*. After several hundred milliseconds, the emission vanishes in a single step. This clearly shows that the surface-immobilized eqFP611 proteins are monomeric, as observed earlier for eqFP611 immobilized in a PVA gel (Wiedenmann et al., 2002). By contrast, Lounis et al. (2001) found multistep bleaching in experiments with DsRed immobilized in agarose gel, implying that DsRed is oligomeric even under high-dilution conditions. Upon disruption of the DsRed tetramer by mutations that disturb the side-chain packing in the interfaces between the monomers, the quantum yield of fluorescence decreases dramatically but can be recovered to a certain extent by introducing further mutations (Campbell et al., 2002). Fortunately, the fluorescence of eqFP611 does not appear to be compromised by monomerization. The photobleaching yield Φ_B of eqFP611 was 1.9×10^{-5} on the PEG surfaces, whereas we had previously reported a smaller value of 3.5×10^{-6} for the PVA preparation (Wiedenmann et al., 2002). Photobleaching depends on the dynamic properties of the molecules, which may differ on the PEG surfaces from those in the gel. Many sol-gels alter dynamic properties and can improve the thermal stability of proteins embedded therein (Gill and Ballesteros, 1998). Moreover, a decrease of Φ_B has been noticed for single molecules embedded in a PMMA gel and related to reduced oxygen transport (Xie, 1998). PVA is known to have a very low oxygen permeability (Brandrup and Immergut, 1989), so that photooxidation in a PVA gel is likely diminished. For DsRed, Φ_B-values between 0.8 and 9.5×10^{-6} have been reported in aqueous buffer solution (Baird et al., 2000; Heikal et al., 2000; Lounis et al., 2001). The spread in these numbers may also reflect the sensitivity of this parameter on the specific environmental conditions in the experiments.

The close interrelation between protein dynamics and

photobleaching and flickering was also apparent in studies of individual eqFP611 molecules dried on a bare glass surface. Interestingly, none of these molecules showed any flickering, as confirmed by the solid squares in Fig. 7 *a*. Rather, they emitted bright fluorescence for several seconds before photobleaching (data not shown). From the analysis of 48 molecules on the glass surface, the bleaching yield was determined as $(1.3 \pm 0.2) \times 10^{-6}$. A similar decrease in photobleaching has been observed by Chirico and co-workers with a GFP mutant (Chirico et al., 2002).

Fluorescence dynamics in solution FCS experiments

Flickering of FPs on sub-ms timescales was first characterized by Haupts and co-workers using EGFP and assigned to proton exchange of the hydroxyl group of Y66 with the external medium (Haupts et al., 1998). Similar results were found with other GFP mutants, suggesting that pH-dependent flickering was ubiquitous among FPs (Heikal et al., 2000; Schwille et al., 2000). In addition to the flickering due to external protonation, GFP mutants were observed to also exhibit an excitation intensity-dependent flickering (Haupts et al., 1998; Heikal et al., 2000; Schwille et al., 2000) and a slow blinking on the second timescale (Dickson et al., 1997).

The red fluorescing FPs, eqFP611 and DsRed, show pH-independent emission and FCS autocorrelation over the pH range 4–11, indicating that proton exchange between the chromophore tyrosine and the external medium is strongly suppressed (Heikal et al., 2000; Wiedenmann et al., 2002). Nevertheless, these red FPs show very clear excitation-dependent flickering (Figs. 2 and 5), as has been reported earlier for DsRed (Heikal et al., 2000; Malvezzi-Campeggi et al., 2001). The similar qualitative behavior of the two proteins suggests a similar underlying photophysical mechanism for the two proteins.

Different kinetic models have been presented in the literature to explain the excitation rate dependence of the flickering. Kinetic schemes that involve only a single light-driven step, as for instance presented by Heikal et al. (2000), cannot explain the intricate power dependence of the dark fraction and the apparent rate coefficient. A kinetic model involving two light-driven processes has been proposed for the yellow-shifted mutants T203Y and T203F of GFP (Schwille et al., 2000). In this case, the second light-driven reaction is the transition from the dark ground state to the dark excited state. This scheme, however, cannot account for the decrease of the dark state fraction for eqFP611 and drFP583 at high excitation rates. For GFP mutant E222Q, a model was proposed in which the protonated dark state is converted to the ground state via light excitation to an unidentified excited state. This model is mathematically equivalent to our model (within the fast approximation), but differs in the assignment of the processes involved (Jung et al., 2000).

Schwille and co-workers (Malvezzi-Campeggi et al., 2001) recently presented a detailed study of flickering of DsRed, in which they introduced three spectroscopically distinguishable states of the chromophore, two of which were assumed to be only weakly fluorescent. *Dim* (instead of dark) states were incorporated because this enabled modeling of the observed decrease of the dark state fraction at higher powers. This treatment, however, cannot explain the dependence of F on the excitation wavelength. *Two* dim states were necessary because the reaction step could not be modeled satisfactorily with a single exponential at higher powers. In our analysis, single-exponential fits gave very reasonable fits to DsRed and eqFP611 data, and there was no clear evidence for discrete exponentials (see Fig. 2). Note that deviations from single exponential ACF at high power can also be caused by photobleaching.

By introducing a scheme with three kinetic states connected by thermal and two light-driven transitions, as shown in Eq. 5, we were able to extract the relevant parameters of the scheme and explain the FCS measurements of the two proteins eqFP611 and drFP583 consistently. Note that we distinguish three conformations, which can be either in the electronic ground (S_0) or first excited state (S_1). The electronic transitions themselves are not considered in this scheme. Within our analysis, the excitation wavelength dependence of both eqFP611 and drFP583 arises from a wavelength-dependent, light-driven transition from the dark state D back to the intermediate state B^*. The quantum yield Φ_{-2} is about twice as large for excitation with 488 nm as compared with excitation at 514/532 nm for both proteins (Table 2). In the analysis, the thermal rate coefficients k_2 and k_{-2} were treated as global parameters, that is, they were forced to be independent of the excitation wavelength. The fit yields similar values for the parameter $P_1 = k_{-1}/\Phi_1$ characterizing the fast equilibrium between the two bright states at the different wavelengths. The most obvious difference between the two red FPs under study is the rate coefficient k_{-2}, which is 6× larger for eqFP611. This parameter is responsible for the faster flicker rate of eqFP611 at low power, which is apparent from the larger temporal separation between the flicker component and the diffusion component in FCS data on eqFP611 (Fig. 2) than on DsRed (Heikal et al., 2000; Malvezzi-Campeggi et al., 2001). While the flicker rate of eqFP611 is larger at small excitation rates, the population of the dark state is smaller compared to drFP583, however. In the parameters in Table 2, this is represented by the larger value of the product of the two parameters $P_1 \cdot P_2$ for eqFP611, which represents the inverse initial slope of the dark state fraction F. Even when using the exact solution, Eq. 7, the fit procedure was unable to provide reliable values for k_{-1}.

In principle, Scheme 5 could be interpreted in a different way: instead of two bright conformations, we could treat B and B^* as the S_0 and S_1 states of the same fluorescent conformation. Then, $\Phi_1 = 1$, and k_{-1} should be the inverse

fluorescence lifetime. For eqFP611, the fluorescence lifetime was measured as 2.5 ns (Wiedenmann et al., 2002), and similar lifetimes in the range of 2.85 to 3.60 ns have been reported for drFP583 (Heikal et al., 2000; Jakobs et al., 2000; Cotlet et al., 2001; Lounis et al., 2001). Thus, identifying the first step in our model as the electronic excitation would imply $k_{-1} \approx 400$ MHz, yielding the same value for P_1. Table 2, however, shows that P_1 is rather in the range of 1 MHz and thus >2 orders-of-magnitude smaller than expected for the electronic transition. Therefore, we can safely conclude that the $B \rightarrow B^*$ transition involves a conformational change and does not merely represent electronic excitation of the chromophore.

Finally, we address the slow flickering on the 10-ms timescale that was seen in the ACFs of single, surface-immobilized eqFP611 molecules. Fig. 2 shows that this process temporally overlaps with the diffusion ACF. This process is also photon-induced because the apparent diffusion coefficient increases with the excitation power. As seen from the data in Fig. 3, the effect is fairly weak for DsRed and much more pronounced for eqFP611 and EGFP. This figure also shows that diffusion coefficients need to be determined by an extrapolation to zero power. Indeed, our diffusion coefficient of 63 $\mu m^2/s$ for EGFP in Table 1 is significantly smaller than the values reported for wild-type GFP and GFP mutants in the literature (Widengren et al., 1999; Jung et al., 2000; Malvezzi-Campeggi et al., 2001). From the diffusion coefficient, we have obtained a volume ratio eqFP611 : EGFP of 2.9 : 1, which is in fair agreement with the assumption that eqFP611 is still somewhat oligomeric at nanomolar concentrations in solution. We emphasize here that the surface-immobilized proteins were monomeric, as verified by single-step bleaching. The similar flickering dynamics observed with the two preparations implies that this is not strongly dependent on the oligomerization state. It is interesting that DsRed diffuses significantly more slowly than eqFP611, in agreement with the data reported by Heikal et al. (2000), which would suggest that this protein forms even larger aggregates. The rotational correlation data in Fig. 4, however, present a different picture: the correlation time of ~16 ns of EGFP agrees with measurements performed earlier on (mutant) GFPs using time-resolved fluorescence anisotropy (Widengren et al., 1999; Heikal et al., 2000; Volkmer et al., 2000). Both red FPs have an identical rotational correlation decay, consistent with tetramer rotation (~64 ns) and the slow (53 ± 8) ns anisotropy decay reported by Heikal et al. (2000). It remains, therefore, unclear why the translational diffusion coefficient of DsRed is markedly smaller than the one of eqFP611.

The detailed characterization of the light-induced dynamics presented here does, unfortunately, not enable us to give a detailed structural interpretation of the processes that are responsible for these phenomena. However, the timescales are consistent with conformational rearrangements around the chromophore, such as light-induced isomerizations of the chromophore and/or the hydrogen-bonding network, as was suggested by structural studies (Brejc et al., 1997) and molecular dynamics simulations (Weber et al., 1999). We are currently pursuing the strategy of modifying the chromophore cage of eqFP611 by site-directed mutagenesis to study the effects on the photodynamics. From this approach, we hope to gain a detailed structural understanding of the photophysical processes in FPs, which should enable us to further improve their usefulness as fluorescent markers in life science applications.

CONCLUSIONS

FCS measurements were performed on solution samples to study the photodynamics of two red FPs, eqFP611 and drFP583. Both proteins show flickering on the sub-ms timescale that depends qualitatively in a similar way on the excitation rate. A three-state model with two light-driven processes was introduced to model the excitation rate and wavelength-dependent flickering of both proteins. A second, markedly slower flickering process was apparent from the power dependence of the diffusional correlation times. The solution studies were complemented by experiments with eqFP611 monomers bound to polymer brush layers on glass surfaces. Fast flickering was observed, consistent with the results from solution FCS. Moreover, slow flickering on the 10-ms timescale was evident from the time traces and ACF analysis. These results give insights into the complex photophysics of FPs but do not yield a structural interpretation. To address structure-dynamics-function relations in FPs, we will perform similar studies using mutants with modified chromophore environments.

APPENDIX: EXCITATION RATE CALIBRATION

The excitation rate k_{ex} is the product of the absorption cross section, which can be expressed by the extinction coefficient at the excitation wavelength, e_l, and the photon flux, which is proportional to the power density p,

$$k_{ex}[s^{-1}] = \frac{\ln(10)10^3}{N_A}\,\varepsilon_\lambda[M^{-1}cm^{-1}] \times \frac{\lambda}{hc}p[Wcm^{-2}]. \quad (A1)$$

Here, N_A denotes Avogadro's number, h represents Planck's constant, and c is the velocity of light. The usual way to determine the power density is to simply divide the measured total power of the excitation light by the area of illumination in the focal plane, which is determined from the diffusion autocorrelation analysis of a fluorescent dye with known diffusion coefficient (Widengren et al., 1994). The illuminated focal area, however, can be larger than the area from which light is collected because the detection volume is restricted by the pinhole. Moreover, light from planes parallel to the focal plane is detected with different efficiencies due to the action of the pinhole. These effects cause problems when comparing measurements with different confocal geometries. Fortunately, the pinhole governs the ratio $\omega = r_0/z_0$ of the lateral radius r_0 and axial dimension z_0 of the confocal volume, as determined by FCS, and we can use the value of ω to obtain an empirical correction factor for the power densities when

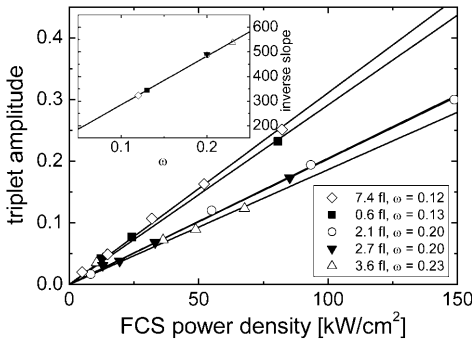

FIGURE 8 Triplet amplitude of rhodamine 6G versus power density (as determined by FCS) for five different observation volumes; (*inset*) inverse slope of the linear fits plotted versus the ratio $\omega = r_0/z_0$.

using different FCS volumes. To show this, we measured the same sample of rhodamine 6G in aqueous solution with five different confocal volumes with ω-values between 0.12 and 0.23 (data not shown). We have used the triplet amplitude of the rhodamine 6G as an inherent indicator of the effective power density in the sample. By plotting the triplet amplitude versus the apparent power density, as determined in the usual way by FCS, we obtained a nicely linear dependence (within our range of the excitation powers) for each of the volumes used, with equal slopes for equal values of ω (Fig. 8). Plotting the inverse slopes of these curves versus ω yields a straight line in the range $\omega = 0.1–0.25$ (Fig. 8, *inset*). This dependence was used to renormalize the power densities obtained from all the different confocal geometries to $\omega = 0.2$, a typical value in standard FCS measurements before calculating the excitation rates according to Eq. A1.

We thank Drs. Christoph Kaether (European Molecular Biology Laboratory, Heidelberg, Germany) and Sergey A. Lukyanov (Russian Academy of Sciences, Moscow, Russia) for kindly providing the EGFP and the drFP583 clones, respectively.

Financial support by the Deutsche Forschungsgemeinschaft (SFB 569 and GRK 328) is gratefully acknowledged.

REFERENCES

Baird, G. S., D. A. Zacharias, and R. Y. Tsien. 2000. Biochemistry, mutagenesis and oligomerization of DsRed, a red fluorescent protein from coral. *Proc. Natl. Acad. Sci. USA*. 97:11984–11989.

Brandrup, J., and E. H. Immergut. 1989. Polymer Handbook. Wiley, New York.

Brejc, K., T. K. Sixma, P. A. Kitts, S. R. Kain, R. Y. Tsien, M. Ormö, and S. J. Remington. 1997. Structural basis for dual excitation and photoisomerization of the *Aequorea victoria* green fluorescent protein. *Proc. Natl. Acad. Sci. USA*. 94:2306–2311.

Campbell, R. E., O. Tour, A. E. Palmer, P. A. Steinbach, G. S. Baird, D. A. Zacharias, and R. Y. Tsien. 2002. A monomeric red fluorescent protein. *Proc. Natl. Acad. Sci. USA*. 99:7877–7882.

Chirico, G., F. Cannone, S. Beretta, A. Diaspro, B. Campanini, S. Bettati, R. Ruotolo, and A. Mozzarelli. 2002. Dynamics of green fluorescent protein mutant 2 in solution, on spin-coated glasses, and encapsulated in wet silica gels. *Protein Sci.* 11:1152–1161.

Cotlet, M., J. Hofkens, S. Habuchi, G. Dirix, M. Van Guyse, J. Michiels, J. Vanderleyden, and F. C. De Schryver. 2001. Identification of different emitting species in the red fluorescent protein DsRed by means of ensemble and single-molecule spectroscopy. *Proc. Natl. Acad. Sci. USA*. 98:14398–14403.

Dickson, R. M., A. B. Cubitt, R. Y. Tsien, and W. E. Moerner. 1997. On/off blinking of single molecules of green fluorescent protein. *Nature*. 388:355–358.

Ehrenstein, D., and G. U. Nienhaus. 1992. Conformational substates in azurin. *Proc. Natl. Acad. Sci. USA*. 89:9681–9685.

Elson, E. L., and D. Magde. 1974. Fluorescence correlation spectroscopy. I. Conceptual basis and theory. *Biopolymers*. 13:1–27.

Frauenfelder, H., S. G. Sligar, and P. G. Wolynes. 1991. The energy landscapes and motions of proteins. *Science*. 254:1598–1603.

Garcia-Parajo, M. F., G. M. J. Segers-Nolten, J. A. Veerman, J. Greve, and N. F. V. Hulst. 2000. Real-time light driven dynamics of the fluorescence emission in single green fluorescent protein molecules. *Proc. Natl. Acad. Sci. USA*. 97:7237–7242.

Gill, I., and A. Ballesteros. 1998. Encapsulation of biologicals within silicate, siloxane, and hybrid sol-gel polymers: an efficient and generic approach. *J. Am. Chem. Soc*. 120:8587–8598.

Haupts, U., S. Maiti, P. Schwille, and W. W. Webb. 1998. Dynamics of fluorescence fluctuations in green fluorescent protein observed by fluorescence correlation spectroscopy. *Proc. Natl. Acad. Sci. USA*. 95: 13573–13578.

He, X., A. F. Bell, and P. J. Tonge. 2002. Synthesis and spectroscopic studies of model red fluorescent protein chromophores. *Org. Lett*. 4: 1523–1526.

Heikal, A. A., S. T. Hess, G. S. Baird, R. Y. Tsien, and W. W. Webb. 2000. Molecular spectroscopy and dynamics of intrinsically fluorescent proteins: Coral Red (dsRed) and Yellow (Citrine). *Proc. Natl. Acad. Sci. USA*. 97:11996–12001.

Helms, V., T. P. Straatsma, and J. A. McCammon. 1999. Internal dynamics of green fluorescent protein. *J. Phys. Chem. B*. 103:3263–3269.

Hermanson, G. T. 1996. Bioconjugate Techniques. Academic Press, London, UK. 386ff.

Hess, S. T., and W. W. Webb. 2002. Focal volume optics and experimental artifacts in confocal fluorescence correlation spectroscopy. *Biophys. J*. 83:2300–2317.

Jakobs, S., V. Subramaniam, A. Schönle, T. M. Jovin, and S. W. Hell. 2000. EGFP and DsRed expressing cultures of *Escherichia coli* imaged by confocal, two-photon and fluorescence lifetime microscopy. *FEBS Lett*. 479:131–135.

Jung, G., S. Mais, A. Zumbusch, and C. Bräuchle. 2000. The role of dark states in the photodynamics of the green fluorescent protein examined with two-color fluorescence excitation spectroscopy. *J. Phys. Chem. A*. 104:873–877.

Jung, G., J. Wiehler, W. Göhde, J. Tittel, T. Basché, B. Steipe, and C. Bräuchle. 1998. Confocal microscopy of single molecules of the green fluorescent protein. *Bioimaging*. 6:54–61.

Kriegl, J. M., A. J. Bhattacharyya, K. Nienhaus, P. Deng, O. Minkow, and G. U. Nienhaus. 2002. Ligand binding and protein dynamics in neuroglobin. *Proc. Natl. Acad. Sci. USA*. 99:7992–7997.

Kruglik, S. G., V. Subramaniam, J. Greve, and C. Otto. 2002. Resonance CARS study of the structure of ''green'' and ''red'' chromophores within the red fluorescent protein DsRed. *J. Am. Chem. Soc*. 124:10992–10993.

Kummer, A. D., C. Kompa, H. Lossau, F. Pollinger-Dammer, M. E. Michel-Beyerle, C. M. Silva, E. J. Bylina, W. J. Coleman, M. M. Yang, and D. C. Youvan. 1998. Dramatic reduction in fluorescence quantum yield in mutants of green fluorescent protein due to fast internal conversion. *Chem. Phys*. 237:183–193.

Kummer, A. D., J. Wiehler, H. Rehaber, C. Kompa, B. Steipe, and M. E. Michel-Beyerle. 2000. Effects of threonine 203 replacements on excited-state dynamics and fluorescence properties of the green fluorescent protein (GFP). *J. Phys. Chem. B*. 104:4791–4798.

Kummer, A. D., J. Wiehler, T. A. Schüttrigkeit, B. W. Berger, B. Steipe, and M. E. Michel-Beyerle. 2002. Picosecond time-resolved fluorescence from blue-emitting chromophore variants Y66F and Y66H of the green fluorescent protein. *Chembiochem*. 3:659–663.

Lamb, D. C., A. Schenk, C. Röcker, C. Scalfi-Happ, and G. U. Nienhaus. 2000. Sensitivity enhancement in fluorescence correlation spectroscopy of multiple species using time-gated detection. *Biophys. J.* 79:1129–1138.

Lounis, B., J. Deich, F. I. Rosell, S. G. Boxer, and W. E. Moerner. 2001. Photophysics of DsRed, a red fluorescent protein, from the ensemble to the single-molecule level. *J. Phys. Chem. B.* 105:5048–5054.

Magde, D., E. L. Elson, and W. W. Webb. 1974. Fluorescence correlation spectroscopy. II. An experimental realization. *Biopolymers.* 13:29–61.

Malvezzi-Campeggi, F., M. Jahnz, K. G. Heinze, P. Dittrich, and P. Schwille. 2001. Light-induced flickering of DsRed provides evidence for distinct and interconvertible fluorescent states. *Biophys. J.* 81:1776–1785.

Matz, M. V., A. F. Fradkov, Y. A. Labas, A. P. Savitsky, A. G. Zaraisky, M. L. Markelov, and K. A. Lukyanov. 1999. Fluorescent proteins from nonbioluminescent Anthozoa species. *Nat. Biotechnol.* 17:969–973.

McMahon, B. H., J. D. Müller, C. A. Wraight, and G. U. Nienhaus. 1998. Electron transfer and protein dynamics in the photosynthetic reaction center. *Biophys. J.* 74:2567–2587.

Nienhaus, G. U., J. D. Müller, B. H. McMahon, and H. Frauenfelder. 1997. Exploring the conformational energy landscape of proteins. *Physica D.* 107:297–311.

Nienhaus, G. U., and R. D. Young. 1996. Protein Dynamics. VCH Publishers, New York. 163–184.

Nienhaus, K., B. Vallone, F. Renzi, J. Wiedenmann, and G. U. Nienhaus. 2003. Crystallization and preliminary x-ray diffraction analysis of the red fluorescent protein eqFP611. *Acta Crystallogr. D.* 59:1253–1255.

Niwa, H., S. Inouye, T. Hirano, T. Matsuno, S. Kojima, M. Kubota, M. Ohashi, and F. I. Tsuji. 1996. Chemical nature of the light emitter of the *Aequorea* green fluorescent protein. *Proc. Natl. Acad. Sci. USA.* 93: 13617–13622.

Olivini, F., S. Beretta, and G. Chirico. 2001. Two-photon fluorescence polarization anisotropy decay on highly diluted solutions by phase fluorometry. *Appl. Spectrosc.* 55:311–317.

Ormö, M., A. B. Cubitt, K. Kallilo, L. A. Gross, R. Y. Tsien, and S. J. Remington. 1996. Crystal structure of the *Aequorea victoria* green fluorescent protein. *Science.* 273:1392–1395.

Peterman, E. G. J., S. Brasselet, and W. E. Moerner. 1999. The fluorescence dynamics of single molecules of green fluorescent protein. *J. Phys. Chem. A.* 103:10553–10560.

Prasher, D. C., V. K. Eckenrode, W. W. Ward, F. G. Prendergast, and M. J. Cormier. 1992. Primary structure of the *Aequorea victoria* green-fluorescent protein. *Gene.* 111:229–233.

Schwille, P., S. Kummer, A. A. Heikal, W. E. Moerner, and W. W. Webb. 2000. Fluorescence correlation spectroscopy reveals fast optical excitation-driven intramolecular dynamics of yellow fluorescent protein. *Proc. Natl. Acad. Sci. USA.* 97:151–156.

Tsien, R. Y. 1998. The green fluorescent protein. *Annu. Rev. Biochem.* 67:509–544.

Voityuk, A. A., M. E. Michel-Beyerle, and N. Rösch. 1998. Structure and rotation barriers for ground and excited states of the isolated chromophore of the green fluorescent protein. *Chem. Phys. Lett.* 296: 269–276.

Volkmer, A., V. Subramaniam, D. J. Birch, and T. M. Jovin. 2000. One- and two-photon excited fluorescence lifetimes and anisotropy decays of green fluorescent proteins. *Biophys. J.* 78:1589–1598.

Wall, M. A., M. Socolich, and R. Ranganathan. 2000. The structural basis for red fluorescence in the tetrameric GFP homolog DsRed. *Nat. Struct. Biol.* 7:1133–1138.

Ward, W. W. 1982. *In* Bioluminescence and Chemoluminescence: Basic Chemistry and Analytical Applications. M. A. DeLuca and W. D. McElroy, editors. Academic Press, New York. 235–242.

Weber, W., V. Helms, J. A. McCammon, and P. W. Langhoff. 1999. Shedding light on the dark and weakly fluorescent states of green fluorescent proteins. *Proc. Natl. Acad. Sci. USA.* 96:6177–6182.

Widengren, J., Ü. Mets, and R. Rigler. 1999. Photodynamic properties of green fluorescent proteins investigated by fluorescence correlation spectroscopy. *Chem. Phys.* 250:171–186.

Widengren, J., R. Rigler, and Ü. Mets. 1994. Triplet-state monitoring by fluorescence correlation spectroscopy. *J. Fluorescence.* 4:255–258.

Wiedenmann, J., C. Elke, K.-D. Spindler, and W. Funke. 2000. Cracks in the β-can: fluorescent proteins from *Anemonia sulcata* (Anthozoa, Actinaria). *Proc. Natl. Acad. Sci. USA.* 97:14091–14096.

Wiedenmann, J., A. Schenk, C. Röcker, A. Girod, K.-D. Spindler, and G. U. Nienhaus. 2002. A far-red fluorescent protein with fast maturation and reduced oligomerization tendency from *Entacmaea quadricolor* (Anthozoa, Actinaria). *Proc. Natl. Acad. Sci. USA.* 99:11646–11651.

Xie, X. S. 1998. Optical studies of single molecules at room temperature. *Annu. Rev. Phys. Chem.* 49:441–480.

Yang, F., L. G. Moss, J. George, and N. Phillips. 1996. The molecular structure of green fluorescent protein. *Nature Biotech.* 14:1246–1251.